32nd Annual International Conference of the IEEE EMBS
Buenos Aires, Argentina, August 31 - September 4, 2010

IEEE EMBC 2010; paper submitted April 23, 2010
Student Paper Competition First-Place Award for Justin Haldar.

Label-Free High-Resolution Imaging of Live Cells With Deconvolved Spatial Light Interference Microscopy

Justin P. Haldar, Zhuo Wang, Gabriel Popescu, Zhi-Pei Liang

***Abstract*— Spatial light interference microscopy (SLIM) is a powerful new quantitative phase optical imaging technique that can be used for studying live cells without the need for exogenous contrast agents. This paper proposes a novel deconvolution-based approach to reconstructing SLIM data, which dramatically improves the visual quality of the images. The proposed deconvolution formulation is tailored to the physics of SLIM imaging of biological samples, and a new fast algorithm is designed for computationally-efficient image reconstruction in this setting. Simulation and experimental results demonstrate that deconvolution can reduce the width of the point-spread function by at least 20%, and can significantly improve the contrast of high-resolution features. Temporally-resolved SLIM imaging with the high spatial resolution enabled by deconvolution provides new opportunities for studying the dynamics of cellular and sub-cellular processes.**

I. Introduction

Optical microscopy is an important tool for studying biology at sub-cellular scales. However, the study of live cells using traditional bright field microscopy is limited by the fact that most cellular structures have little absorption and are virtually transparent to visible light. While it is possible to increase contrast by using exogenous contrast agents (i.e., staining/labeling cellular structures with dyes or fluorophores), the use of such agents can require complicated sample preparation and/or can interfere with the viability of live cells [1]. Phase contrast (PC) and differential interference contrast (DIC) microscopy offer the ability to visualize sub-cellular features of live cells without labels, using the optical phase shift of the light passing through a sample (a function of the sample's thickness and refractive index) as an endogenous contrast mechanism. Quantitative phase imaging (QPI) represents an evolution of PC and DIC techniques that can make precise measurements of the optical phase shift through a sample, which can subsequently be used to infer a variety of important biological parameters [2].

Spatial light interference microscopy (SLIM) is a new QPI method that offers significantly enhanced sensitivity and resolving power relative to previously reported QPI systems [3], [4]. However, like other optical microscopy techniques, the spatial resolution of SLIM is generally limited by diffraction and imperfections in the microscope system. In this work, we demonstrate that the use of a deconvolution approach [5] to reconstruct the original optical field significantly enhances SLIM images, and can help make SLIM an even more powerful tool for understanding the morphology and dynamics of live cells.

Submitted April 23, 2010. This work was supported in part by research grants NIH-P41-EB001977-21, NIH-P41-RR023953-01, and NSF-CBET-07-30623.

J. Haldar, Z. Wang, G. Popescu, and Z.-P. Liang are with the Department of Electrical and Computer Engineering and the Beckman Institute for Advanced Science and Technology, University of Illinois at Urbana-Champaign. haldar@uiuc.edu

II. Problem Formulation

We will focus on two-dimensional imaging of thin samples in this work; a more complete discussion of the physics of SLIM can be found elsewhere [3]. We denote the complex-valued optical field of interest as $U(x,y)$, where x and y are spatial variables. We assume that $|U(x,y)|$ is constant throughout the field of view, due to the near-transparency of the sample, such that $U(x,y)$ can be written as $U(x,y) = \alpha e^{i\Psi(x,y)}$, where α is the magnitude of the field. Without loss of generality, we will assume that the magnitude of $U(x,y)$ is normalized to 1.

The optical field observed at the detector plane $O(x,y)$ is a degraded version of $U(x,y)$. This degradation process is well-modeled using the convolution relationship

$$O(x,y) = \iint h(x-s, y-t)\, U(s,t) ds dt, \qquad (1)$$

where $h(x,y)$ is the point-spread function (PSF) of the microscope. We will denote the magnitude and phase of $O(x,y)$ as $M(x,y)$ and $\Phi(x,y)$, respectively. SLIM uses interferometry to measure the phase $\Phi(x,y)$,

while the magnitude $M(x,y)$ of the field is not measured.[1] In practice, an array of charge-coupled device (CCD) detectors is used to record the interferometric data, such that we have access to samples of $\Phi(x,y)$ on the Cartesian grid of points determined by the spatial locations of the CCD detectors.

The goal of the present work is to recover $U(x,y)$ from the sampled values of $\Phi(x,y)$. The deconvolution procedure is quite different for SLIM than it is for conventional deconvolution microscopy [5], due to the direct measurement of phase information rather than the intensity information that is acquired in more conventional microscopy applications.

III. Proposed Method

The proposed method consists of two steps. The first step involves the determination of the PSF of the microscope. We measure the PSF by SLIM imaging of sub-resolution microbeads, which are used to represent point sources [5].

In the second step, we use the measured PSF and Eq. (1) to recover a high-resolution estimate of $U(x,y)$ from $\Phi(x,y)$. For practical implementation, we consider a discretization of Eq. (1):

$$\mathbf{m} \odot e^{i\boldsymbol{\Phi}} = \mathbf{H} e^{i\boldsymbol{\Psi}}, \tag{2}$$

where $\odot$ denotes the Hadamard product (element-by-element multiplication), and $\mathbf{H}$ is a Toeplitz-block-Toeplitz matrix representing two-dimensional convolution with the PSF. The vectors $\mathbf{m}$, $e^{i\boldsymbol{\Phi}}$, and $e^{i\boldsymbol{\Psi}}$ contain spatial samples of $M(x,y)$, $e^{i\Phi(x,y)}$, and $U(x,y) = e^{i\Psi(x,y)}$, respectively, with the spatial sampling locations defined by the locations of the CCD detectors. Note that $\mathbf{H}$ and $\boldsymbol{\phi}$ in Eq. (2) are assumed to be known, while $\mathbf{m}$ and $\boldsymbol{\psi}$ are unknowns that will be estimated.

Due to noise and modeling error, it is not always possible to find a solution for which Eq. (2) holds exactly, and a frequently-used approach is to identify parameter estimates that match the observed data as closely as possible. In traditional deconvolution microscopy [5], it is common to use a data-fidelity criterion that models the Poisson statistics of photon-limited optical imaging. In contrast to photon-limited scenarios, SLIM has intrinsically high signal-to-noise ratio due to the use of white-light illumination, and the dominant sources of measurement errors for SLIM are small instrumental instabilities. As a result, we adopt a least-squares data-fidelity criterion because it leads to efficient computations:

$$\left\{\hat{\mathbf{m}}, \hat{\boldsymbol{\psi}}\right\} = \arg\min_{\substack{\mathbf{m},\boldsymbol{\psi} \\ \mathbf{m}\geq\mathbf{0}}} \left\| \mathbf{m} \odot e^{i\boldsymbol{\Phi}} - \mathbf{H} e^{i\boldsymbol{\Psi}} \right\|_{\ell_2}^2, \tag{3}$$

where $\|\cdot\|_{\ell_2}^2$ computes the sum-of-squares. In practice, however, the problem in Eq. (3) is very ill-posed, in the sense that the inverse mapping from $\Phi(x,y)$ to $\Psi(x,y)$ through Eq. (3) is unstable with respect to small perturbations of $\Phi(x,y)$. As a result, it is necessary to use additional constraints to obtain meaningful results. We propose to estimate $\mathbf{m}$ and $\boldsymbol{\psi}$ by solving the following penalized nonlinear least-squares problem:

$$\left\{\hat{\mathbf{m}}, \hat{\boldsymbol{\psi}}\right\} = \arg\min_{\substack{\mathbf{m},\boldsymbol{\psi} \\ \mathbf{m}\geq\mathbf{0}}} \left\| \mathbf{m} \odot e^{i\boldsymbol{\Phi}} - \mathbf{H} e^{i\boldsymbol{\Psi}} \right\|_{\ell_2}^2 + \lambda R\left(e^{i\boldsymbol{\Psi}}\right), \tag{4}$$

where $R\left(e^{i\boldsymbol{\Psi}}\right)$ is a regularization functional that penalizes unlikely reconstructions, and λ is a regularization parameter. In particular, we assume that the true $U(x,y)$ is relatively smooth, and thus encourage smooth reconstructions using

$$R\left(e^{i\boldsymbol{\Psi}}\right) = \left\| \begin{bmatrix} \mathbf{D}_x \\ \mathbf{D}_y \end{bmatrix} e^{i\boldsymbol{\Psi}} \right\|_{\ell_2}^2,$$

where $\mathbf{D}_x$ and $\mathbf{D}_y$ are matrices that use finite-differences to approximate spatial differentiation along x and y, respectively.

A. Algorithm

Equation (4) represents a nonlinear, nonconvex optimization problem, and does not have a closed form solution. However, for a fixed value of $\boldsymbol{\psi}$, the optimal $\mathbf{m}$ does have a closed form solution:

$$\begin{aligned} \hat{\mathbf{m}} &= \arg\min_{\mathbf{m}\geq\mathbf{0}} \left\| \mathbf{m} \odot e^{i\boldsymbol{\Phi}} - \mathbf{H} e^{i\boldsymbol{\Psi}} \right\|_{\ell_2}^2 + \lambda R\left(e^{i\boldsymbol{\Psi}}\right) \\ &= \left[e^{-i\boldsymbol{\Phi}} \odot \mathbf{H} e^{i\boldsymbol{\Psi}} \right]_+, \end{aligned}$$

where $[\mathbf{z}]_+ = \mathrm{real}(\mathbf{z}) \odot \mathbf{1}_{\{\mathrm{real}(\mathbf{z})>0\}}$, and $\mathbf{1}_{\{\mathrm{real}(\mathbf{z})>0\}}$ is an indicator function that indicates the entries of $\mathbf{z}$ where $\mathrm{real}(\mathbf{z})$ is positive. As a result of this closed form solution, we can use the variable projection framework [6] to instead find a solution to

$$\hat{\boldsymbol{\psi}} = \arg\min_{\boldsymbol{\psi}} \left\| \left[e^{-i\boldsymbol{\Phi}} \odot \mathbf{H} e^{i\boldsymbol{\Psi}} \right]_- \right\|_{\ell_2}^2 + \lambda R\left(e^{i\boldsymbol{\Psi}}\right), \tag{5}$$

where $[\mathbf{z}]_- = \mathbf{z} - [\mathbf{z}]_+$. The variable projection framework ensures that Eq. (5) has the same optimal solution for $\hat{\boldsymbol{\psi}}$ as Eq. (4), and the use of variable projection generally reduces the number of optimization variables,

[1] A measurement of the magnitude would require instrument modification, and would have limited information content due to the transparency of the sample.

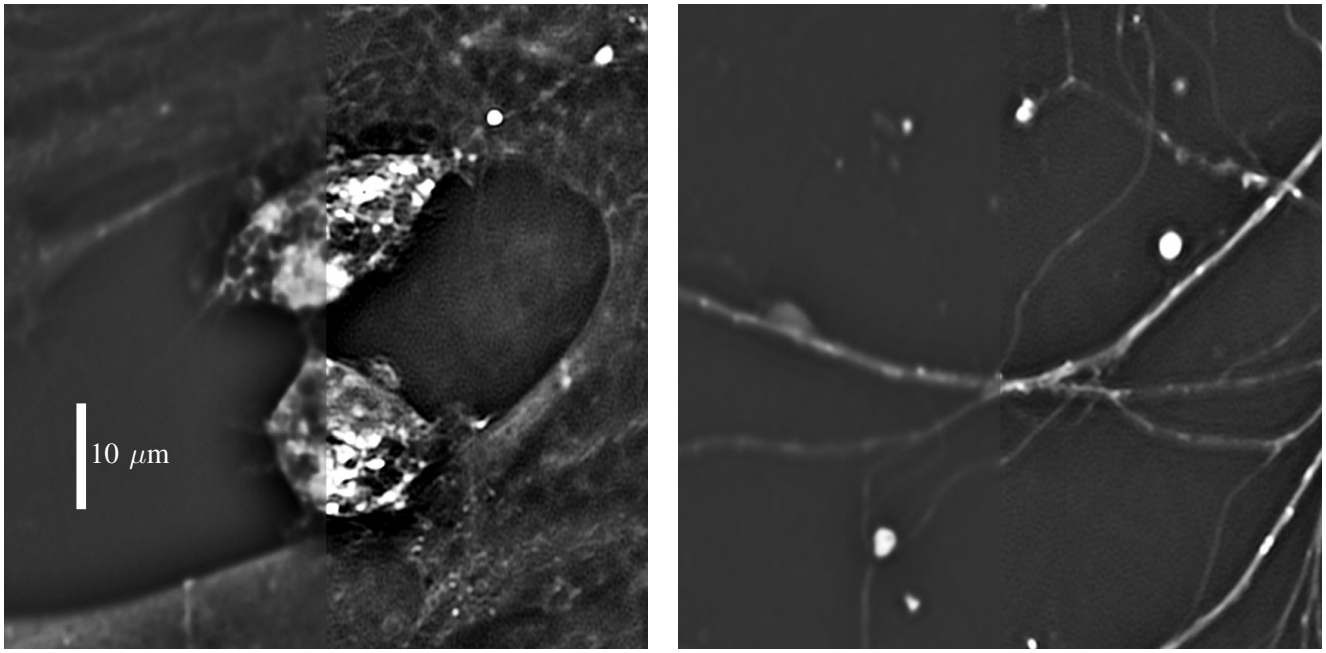

(a) Mixed glial cultures (b) Neuron cultures

Fig. 1. SLIM snapshot images of cell cultures derived from postnatal (P1-P2) Long-Evans BluGill rats. (a) Mixed glial cultures from bilateral dissection of the ventral hypothalamus. (b) Primary hippocampal neuron cultures from the CA1-CA3 region of the hippocampus. The left side of each image shows the original observed phase, while the right side shows the phase after application of the proposed deconvolution-based processing. The 10 μm scale bar is valid for both images.

reduces computational complexity, and improves the convergence rate of iterative algorithms [6].

We use the Polak-Ribiere nonlinear conjugate gradient (NCG) method [7] to find a local critical point of Eq. (5), where the gradient of Eq. (5) with respect to $\boldsymbol{\psi}$ is given by

$$\begin{aligned}\mathbf{g}_{\boldsymbol{\psi}} = & \\ & -2\sin(\boldsymbol{\psi}) \odot \left(\mathbf{H}_i^H \mathrm{imag}\left(e^{-i\boldsymbol{\Phi}} \odot \mathbf{H} e^{i\boldsymbol{\psi}}\right)\right) \\ & +2\cos(\boldsymbol{\psi}) \odot \left(\mathbf{H}_r^H \mathrm{imag}\left(e^{-i\boldsymbol{\Phi}} \odot \mathbf{H} e^{i\boldsymbol{\psi}}\right)\right) \\ & -2\sin(\boldsymbol{\psi}) \odot \left(\mathbf{H}_r^H \mathbf{Z} \mathrm{real}\left(e^{-i\boldsymbol{\Phi}} \odot \mathbf{H} e^{i\boldsymbol{\psi}}\right)\right) \\ & -2\cos(\boldsymbol{\psi}) \odot \left(\mathbf{H}_i^H \mathbf{Z} \mathrm{real}\left(e^{-i\boldsymbol{\Phi}} \odot \mathbf{H} e^{i\boldsymbol{\psi}}\right)\right) \\ & +2\lambda \mathrm{imag}\left(e^{-i\boldsymbol{\psi}} \odot \left(\mathbf{D}_x^H \mathbf{D}_x e^{i\boldsymbol{\psi}} + \mathbf{D}_y^H \mathbf{D}_y e^{i\boldsymbol{\psi}}\right)\right),\end{aligned}$$

with

$$\mathbf{H}_i = \mathrm{imag}\left(\mathrm{diag}\left(e^{-i\boldsymbol{\Phi}}\right)\mathbf{H}\right),$$

$$\mathbf{H}_r = \mathrm{real}\left(\mathrm{diag}\left(e^{-i\boldsymbol{\Phi}}\right)\mathbf{H}\right),$$

and

$$\mathbf{Z} = \mathrm{diag}\left(\mathbf{1}_{\{\mathrm{real}(e^{-i\boldsymbol{\Phi}} \odot \mathbf{H} e^{i\boldsymbol{\psi}}) < 0\}}\right).$$

In practice, due to the local convergence of NCG, it is important to initialize the algorithm well. We have found that a reasonable starting point can be obtained by assuming $\mathbf{m}$ in Eq. (4) is constant, and by ignoring the constraint that $U(x,y)$ has constant magnitude. In this case, Eq. (4) can be reformulated as

$$\hat{\mathbf{u}} = \arg\min_{\mathbf{u}} \left\| e^{i\boldsymbol{\Phi}} - \mathbf{H}\mathbf{u} \right\|_{\ell_2}^2 + \lambda R(\mathbf{u}), \qquad (6)$$

where $\mathbf{u}$ is a complex vector of spatial samples of $U(x,y)$, and an initial guess for $\boldsymbol{\psi}$ is obtained from extracting the phase from $\hat{\mathbf{u}}$. In practice, we have observed that the phase of $\hat{\mathbf{u}}$ and the final estimated phase using Eq. (4) are generally quite similar. The benefit to using Eq. (6) for initialization is that the solution is linear and has the closed form

$$\hat{\mathbf{u}} = \left(\mathbf{H}^H\mathbf{H} + \lambda\mathbf{D}_x^H\mathbf{D}_x + \lambda\mathbf{D}_y^H\mathbf{D}_y\right)^{-1}\mathbf{H}^H e^{i\boldsymbol{\Phi}}. \qquad (7)$$

The matrices in this expression all have Toeplitz-block-Toeplitz structure, which means that the optimal $\hat{\mathbf{u}}$ can be found using standard Toeplitz/circulant solvers that leverage the fast Fourier transform to considerably improve computational efficiency [8], [9].

IV. Results and Discussion

In all experiments, SLIM imaging was performed with a white-light source (wavelengths between 400 and 700 nm), with a 1040×1388 CCD array sampling uniformly over 75 μm × 100 μm field of view.

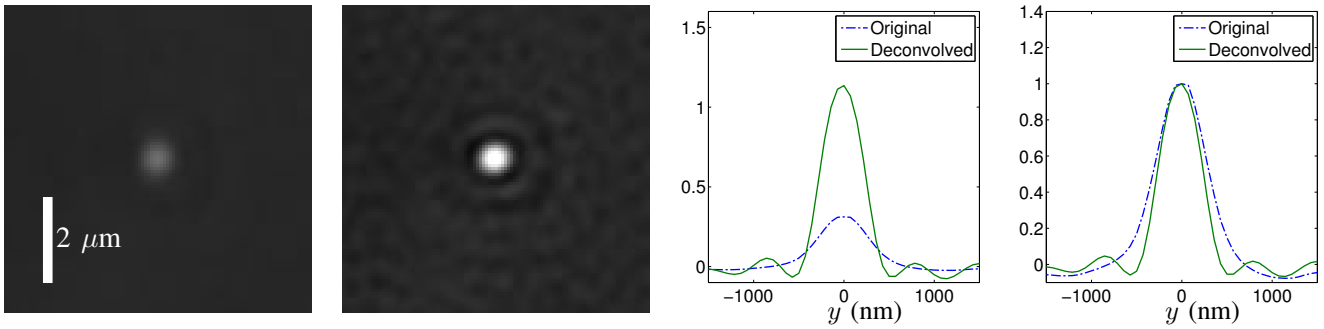

(a) Original Image (b) Deconvolved Image (c) Bead Profiles (d) Normalized Bead Profiles

Fig. 2. SLIM phase images of 200 nm polystyrene beads (a) before and (b) after deconvolution-based reconstruction. (c) Profiles through the centers of these phase images illustrate that the deconvolution process increases the peak phase of the beads, as expected for a higher-resolution image. (d) After normalization of the profiles, it is apparent that the spatial resolution has also improved, with the full-width-at-half-maximum approximately 20% smaller for the deconvolved result.

Figure 1 shows live cell imaging results obtained using the proposed method, which demonstrate significant visual enhancement relative to the original blurry images recorded by the CCD array. Due to the temporal resolutions possible with SLIM (on the order of several Hz), it is possible to clearly visualize a number of different sub-cellular processes, including the dynamics of the actin network and various transport processes.

Imaging of 200 nm microbeads was performed to analyze the improvement in resolution with the proposed approach, and a representative example is shown in Fig. 2. As the figure illustrates, the deconvolution method successfully increases the resolution, with a reduction in the full-width-at-half-maximum (FWHM) of the the PSF by approximately 20%. This 20% reduction in the FWHM is consistent with additional numerical simulations with an ideal point-source (not shown), which suggest that the resolution has improved from 544 nm down to 430 nm using deconvolution.

The regularization parameter λ for all reconstructions was chosen based on a singular-value analysis so that the condition number κ of the matrix inversion in Eq. (7) was equal to 500 (significantly smaller than 10^{14}, which was the condition number of the unregularized problem). Figure 3 illustrates the noise-amplification effects of using smaller values of λ.

V. Conclusions

This paper proposed a deconvolution-based approach for reconstructing SLIM images, using a novel formulation that was specifically tailored to SLIM imaging and a new fast algorithm to solve the resulting optimization problem. Simulation and experimental results indicate significant resolution enhancement with the proposed approach, with important implications for label-free high-resolution imaging of live cells.

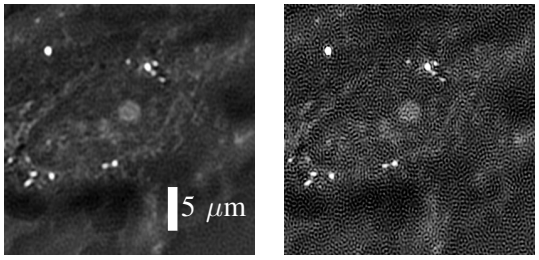

(a) $\kappa = 500$ (b) $\kappa = 50\,000$

Fig. 3. Reconstruction results using different regularization parameters. κ refers to the condition number of Eq. (7).

References

[1] D. J. Stephens and V. J. Allan, "Light microscopy techniques for live cell imaging," *Science*, vol. 300, pp. 82–86, 2003.

[2] G. Popescu, "Quantitative phase imaging of nanoscale cell structure and dynamics," in *Methods in Cell Biology*, B. Jena, Ed. Elsevier Inc., 2008, vol. 90, pp. 87–115.

[3] Z. Wang, L. J. Millet, H. Ding, M. Mir, S. Unarunotai, J. A. Rogers, M. U. Gillette, and G. Popescu, "Spatial light interference microscopy (SLIM)," *Preprint*.

[4] Z. Wang, I. S. Chun, X. Li, Z.-Y. Ong, E. Pop, L. Millet, M. Gillette, and G. Popescu, "Topography and refractometry of nanostructures using spatial light interference microscopy," *Opt. Lett.*, vol. 35, pp. 208–210, 2010.

[5] J.-B. Sibarita, "Deconvolution microscopy," *Adv. Biochem. Engin./Biotechnol.*, vol. 95, pp. 201–243, 2005.

[6] G. Golub and V. Pereyra, "Separable nonlinear least squares: the variable projection method and its applications," *Inverse Probl.*, vol. 19, pp. R1–R26, 2003.

[7] W. H. Press, S. A. Teukolsky, W. T. Vetterling, and B. P. Flannery, *Numerical recipes in C*, 2nd ed. Cambridge: Cambridge University Press, 1992.

[8] R. H. Chan and M. K. Ng, "Conjugate gradient methods for Toeplitz systems," *SIAM Rev.*, vol. 38, pp. 427–482, 1996.

[9] C. R. Vogel, *Computational methods for Inverse Problems*. Philadelphia: SIAM, 2002.